Biosensors and Bioelectronics 137 (2019) 133–139

Contents lists available at ScienceDirect

Biosensors and Bioelectronics

journal homepage: www.elsevier.com/locate/bios

Introducing bifunctional metal-organic frameworks to the construction of a novel ratiometric fluorescence sensor for screening acid phosphatase activity

Siqi Li[a], Xue Hu[a], Qiumeng Chen[a], Xiaodan Zhang[a], Hongxiang Chai[b,*], Yuming Huang[a,**]

[a] The Key Laboratory of Luminescence and Real-time Analytical Chemistry, Ministry of Education, College of Chemistry and Chemical Engineering, Southwest University, Chongqing, 400715, China

[b] Key Laboratory of Eco-environments in Three Gorges Reservoir Region (Ministry of Education), School of Urban Construction and Environmental Engineering, Chongqing University, Shapingba, Chongqing, 400045, China

ARTICLE INFO

Keywords:
Metal-organic frameworks
Biomimetic catalyst
Luminescent sensor
Ratiometric fluorescence
Acid phosphatase
Logic gate

ABSTRACT

Restricted to single sensing mechanisms, most luminescent metal-organic framework (LMOF)-based sensors were constructed for detection of limited targets. Here, a new biosensor is described for screening acid phosphatase (ACP) activity via bifunctional NH_2-MIL-101 MOFs acting as both fluorescent indicator and biomimetic catalyst. NH_2-MIL-101 possesses an inherent fluorescence emission at 456 nm (F_{456}). As a peroxidase-like nanozyme, it catalyzes oxidation of *o*-phenylenediamine (OPD) by H_2O_2 to generate fluorescent 2,3-diaminophenazine with the maximum emission at 556 nm (F_{556}). Upon introducing NH_2-MIL-101 into a mixture of OPD and H_2O_2, F_{456} is quenched, while F_{556} increases. The ACP sensing is based on pyrophosphate ion (PPi) mediated fluorescence tuning of the NH_2-MIL-101/OPD/H_2O_2 system. PPi inhibits the NH_2-MIL-101 catalytic ability by specific binding to its Fe center, while ACP addition recovers the activity by hydrolyzing PPi. Upon addition of PPi and ACP into the NH_2-MIL-101/OPD/H_2O_2 system, a ratiometric luminescence signal (F_{556}/F_{456}) is obtained, and a ratiometric fluorescent sensor can be developed for the sensitive detection of PPi and for screening ACP activity. Plots of F_{556}/F_{456} vs. ACP concentration were linear over 0.01–30 U/L, with a detection limit of 0.005 U/L. The proposed sensor was successfully used for ACP detection in serum samples. This ratiometric fluorescence assay will open new applications for LMOF-based biosensors.

1. Introduction

Metal-organic frameworks (MOFs) are highly porous crystalline materials built from the self-assembly of metal ions/clusters and organic linkers. Their specific merits have stimulated explosive developments in various fields (Zhou and Kitagawa, 2014; Nath et al., 2016; Jiao et al., 2018; Gkaniatsou et al., 2017). Recently, luminescent MOF (LMOF)-based chemical sensors have captured a growing interest (Kreno et al., 2012; Yi et al., 2016; Lei et al., 2014; Allendorf et al., 2009; Cui et al., 2012; Hu et al., 2014). MOF structural predictability and synthetic flexibility make them a promising platform for the construction of diverse solid-state luminescent materials and functionalization of desirable luminophores (Allendorf et al., 2009; Cui et al., 2012; Hu et al., 2014). Meanwhile, the sustainable pores within LMOFs facilitate pre-concentration of target guest molecules and increase guest-host interactions for more sensitive chemical sensing (Kreno et al., 2012; Yi et al., 2016; Allendorf et al., 2009; Cui et al., 2012; Hu et al., 2014). LMOFs-based sensors have been developed by monitoring their intrinsic luminescence. However, most of LMOFs-based sensors exhibit substantial luminescence responses to only a few varieties of guests, such as volatile organic compounds, ionic species, and small molecules (e.g., H_2S, amines and nitroaromatic explosives) (Kreno et al., 2012; Yi et al., 2016; Hu et al., 2014). Detection of biological molecules has been unusual because the sensing mechanism has been restricted to direct guest-host interactions, which are highly dependent on the electronic nature of the guests. Only guest molecules with good electron donor or acceptor capabilities can be readily detected. Furthermore, signal transductions in LMOFs-based sensors are mainly realized by luminescent quenching, or, occasionally, enhancement (Kreno et al., 2012; Yi et al., 2016; Hu et al., 2014). Such a single sensing mechanism often limits further applications to real samples. Therefore, continuous efforts are expected to propose alternative

* Corresponding author.
** Corresponding author.
E-mail addresses: chaihx@cqu.edu.cn (H. Chai), ymhuang@swu.edu.cn (Y. Huang).

https://doi.org/10.1016/j.bios.2019.05.010
Received 25 November 2018; Received in revised form 5 April 2019; Accepted 4 May 2019
Available online 07 May 2019
0956-5663/

sensing strategies for LMOFs-based sensors to expand their applications. The introduction of additional host-guest interactions for luminescent responses in LMOFs-based sensors may be an effective alternative.

MOFs with unsaturated metallic nodes, such as Fe-based MOFs, have biomimetic catalytic activity (Li et al., 2018; Ai et al., 2013; Feng et al., 2012). When coupled with H_2O_2 and enzyme-linked substrates, Fe–O clusters in those MOFs can activate H_2O_2 to produce ·OH radicals via a Fenton-like route, which readily oxidize the substrates into visually detectable products. Thus, various colorimetric assays for H_2O_2, small biomolecules, and biomacromolecules have been reported (Li et al., 2018; Ai et al., 2013; Feng et al., 2012). From the simultaneous use of the excellent luminescence and biomimetic catalytic properties of MOFs, it is therefore possible to form LMOFs-based biosensors by introducing additional host-guest interactions.

Acid phosphatases (ACP) are enzymes that hydrolyze phosphate esters in acid media, and, clinically, both qualitative and quantitative ACP evaluations are important (Kong and Byun, 2013; Seki et al., 2004; Yam, 1974). Methods for ACP detection have included colorimetric (Xu et al., 2014; Deng et al., 2017) and fluorescence assays (Xu et al., 2014; Qian et al., 2015; Wang et al., 2016; Sun et al., 2015; Huang et al., 2016). The fluorescence assay has higher sensitivity, and is easy to perform at low cost (Xu et al., 2014; Sun et al., 2015; Qian et al., 2015; Huang et al., 2016). Various fluorescent (FL) probes have been developed for ACP sensing, including squaraine dyes (Xu et al., 2014), carbon quantum dots (Qian et al., 2015), cadmium telluride quantum dots (Wang et al., 2016), gold nanoclusters (Sun et al., 2015), copper nanoclusters (Huang et al., 2016) and so on. However, these assays are based on a single-emission detective mode, which could suffer from environmental or background factors or other molecules with similar electronic properties. The ratiometric way is more accurate and effective because it is capable of amplifying the signal readout and providing a built-in correction (Lee et al., 2015; Zhao et al., 2017; Teng et al., 2015; Liu et al., 2016). In addition, the change of ratiometric value enables distinct fluorescent color changes to be visually observed (Gong et al., 2017; Srikun et al., 2008). However, to the best of our knowledge, no ratiometric fluorescence sensor has been developed for screening ACP activity.

Here, a LMOF-based biosensor for ACP was developed by using bifunctional NH_2-MIL-101 MOFs that are both fluorescence indicators and biomimetic catalysts. The NH_2-MIL-101 possesses an inherent fluorescence with the maximum emission at 456 nm (F_{456}). As a peroxidase-like nanozyme, it also catalyzes H_2O_2 oxidation of the enzyme-linked substrate *o*-phenylenediamine (OPD) to generate fluorescent 2,3-diaminophenazine (DAP) with maximum emission at 556 nm (F_{556}). As shown in Scheme 1, when NH_2-MIL-101 is mixed with OPD and H_2O_2, its fluorescence is quenched via the inner-filter effect (IFE), while F_{556} increases (process ①). ACP sensing is thus based on pyrophosphate ion-(PPi) mediated FL tuning of the NH_2-MIL-101/OPD/H_2O_2 system. Specifically, PPi can inhibit the NH_2-MIL-101 catalysis of OPD oxidation (process ②) because it binds to the NH_2-MIL-101 Fe center. ACP restores the catalysis by hydrolyzing PPi (process ③). Hence, the addition of PPi and ACP to the NH_2-MIL-101/OPD/H_2O_2 system creates a ratiometric luminescence signal F_{556}/F_{456} that detects PPi and screens for ACP activity. ACP detection and activity screening was demonstrated in real serum samples.

2. Experimental

2.1. Chemicals

All chemicals were analytical grade and used without further purification. 2-Amino-benzenedicarboxylic acid (NH_2-BDC) was purchased from TCI (Shanghai, China). Acid phosphatase (ACP), glucose oxidase (GOx), human serum albumin (HSA), and immunoglobulin G (IgG) were purchased from Sigma-Aldrich (Shanghai, China). Serine (Ser), alanine (Ala), histidine (His), arginine (Arg), aspartic acid (Asp), cysteine (Cys) and tryptophan (Try) were purchased from Shanghai Kangda Biotechnology Co. Ltd. (Shanghai, China). Glucose (Glu) and fructose (Fru) were purchased from Sinopharm Chemical Reagent Co. (Shanghai, China). *N*,*N*-dimethylformamide (DMF), ferric chloride hexahydrate ($FeCl_3{\cdot}6H_2O$), OPD, and sodium pyrophosphate were supplied by Chongqing Taixin Chemical Co. Ltd. (Chongqing, China). Human serum samples were obtained from a local hospital (the Ninth Hospital of Chongqing, Beibei). The stock solution of OPD was freshly prepared daily with ethanol, and the other solutions were prepared using ultra-pure water.

2.2. Apparatus

Scanning electron microscope (SEM) images were acquired on a Hitachi S-4800 field emission electron microscope (Hitachi, Japan), operated at an accelerating voltage of 25 kV. X-ray diffraction (XRD) patterns of the MOFs were collected by using a TD-3500 X-ray diffractometer (Dandong, China), equipped with a nickel-filtered 0.15406-nm Cu K*α* source operated at 20 mA and 30 kV. Fourier transform infrared (FT-IR) spectra were acquired with a Tenson 27 FT-IR

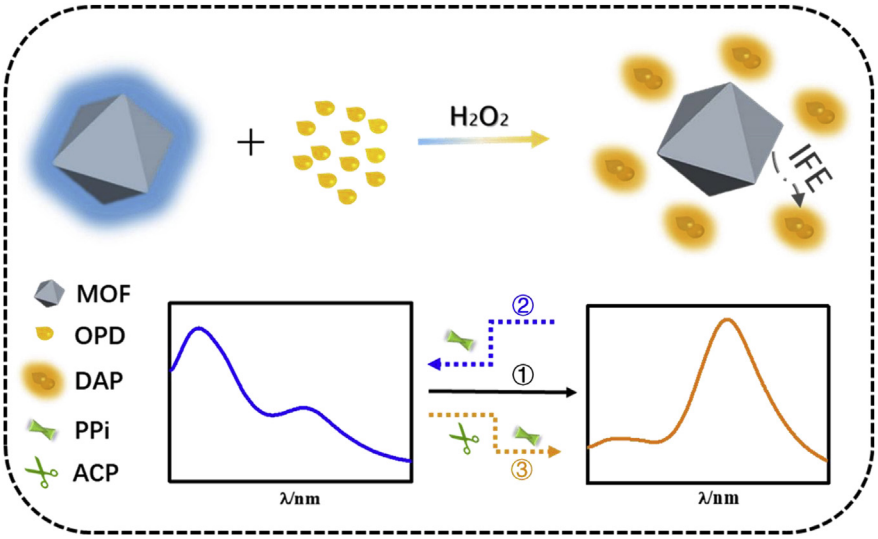

Scheme 1. Schematic of the inner-filter effect between NH_2-MIL-101 and DAP in the NH_2-MIL-101/OPD/H_2O_2 system, and ACP sensing via PPi-mediated FL tuning of the NH_2-MIL-101/OPD/H_2O_2 system.

spectrometer (Bruker, Germany). Zeta potentials were measured with a Malvern Instruments Zetasizer Nano-ZS (Malvern, UK). UV–vis absorption spectra were acquired on a UV-2450 spectrophotometer (Shimadzu, Japan). Fluorescence spectra were acquired with a Hitachi F-2700 spectrophotometer (Hitachi, Japan).

2.3. Synthesis of NH_2-MIL-101 MOFs

MOFs were prepared as previously reported (Bauer et al., 2008; Kathryn et al., 2009). Briefly, the NH_2-MIL-101 was synthesized by hydrothermal treatment of a mixture of $FeCl_3{\cdot}6H_2O$, NH_2-BDC, and DMF with a molar ratio of 2:1:156 at 110 °C for 24 h. MIL-101 was prepared similarly, except that NH_2-BDC was replaced by BDC. The MOFs were collected by centrifugation, washed with DMF and ethanol several times, and dried thoroughly at 60 °C.

2.4. OPD oxidation by H_2O_2 in the presence of NH_2-MIL-101 or MIL-101

Initially, 0.1 mL of 250 μg/mL NH_2-MIL-101 or MIL-101 was added to 4.4 mL of acetate buffer (0.2 M, pH 4.0). Then, 0.25 mL of 3 mM H_2O_2 and 0.25 mL of 0.1 M OPD were introduced. After an incubation of the mixtures at 37 °C for 20 min, 430–650 nm fluorescence spectra (410 nm excitation) were recorded. The excitation and emission slit widths were 5 nm and 10 nm, respectively.

2.5. Detection of PPi and ACP

A series of PPi solutions with different concentrations over the range 0–25 μM were added to 0.1 mL of 250 μg/mL NH_2-MIL-101, 0.25 mL of 3 mM H_2O_2, and 0.25 mL of 0.1 M OPD in acetate buffer (0.2 M, pH 4.0). After incubation at 37 °C for 20 min, 430–650 nm fluorescence spectra at 410 nm excitation were recorded. ACP at different concentrations ranging over 0–100 U/L was mixed with 10 μM PPi in 1 mL of acetate buffer (10 mM, pH 5.0). After incubation at 37 °C for 60 min, the mixture was added to 0.1 mL of 250 μg/mL NH_2-MIL-101, 0.25 mL of 3 mM H_2O_2, and 0.25 mL of 0.1 M OPD in acetate buffer (0.2 M, pH 4.0). These solutions were then treated as described above for PPi.

2.6. Assay for ACP in human serum samples

Human serum samples were treated in 30-kDa Amicon ultrafiltration cells at 3000 rpm for 30 min. Then, the filtrate was diluted 100 times with acetate buffer for ACP detection in the serum, as described above.

3. Results and discussion

3.1. Characterization of NH_2-MIL-101

The SEM image in Fig. 1A indicates that the synthesized NH_2-MIL-101 had an octahedral morphology with a diameter around 400 nm. The XRD pattern in Fig. 1B indicated that the characteristic peaks of NH_2-MIL-101 were consistent with a simulation of MIL-101; a pure MOF phase was indicated by the absence of other peaks. Based on the NH_2-MIL-101 chemical structure (Bauer et al., 2008; Stavitski et al., 2011) (Scheme S1), the 770 cm^{-1} peak in the FT-IR spectrum (Fig. 1C), was attributed to C–H bending vibrations in benzene (Li et al., 2017). The peaks at 1431 cm^{-1} and 1578 cm^{-1} were asymmetric and symmetric vibrations of carboxyl groups in the frameworks (Wu et al., 2013). The 1656 cm^{-1} peak for C = O stretching was from guest DMF CONH bands (Barbosa et al., 2017). Peaks at 3462 cm^{-1} and 3372 cm^{-1} were attributed to asymmetrical and symmetrical amine stretching (Zhang et al., 2016). The fluorescence spectrum of NH_2-MIL-101 (Fig. 1D) exhibits an intense fluorescence emission at 456 nm, which originated from its organic linker NH_2-BDC (Fig. S1D). To verify this, MIL-101 was prepared under the same conditions as NH_2-MIL-101, except that NH_2-BDC was replaced with BDC. The MIL-101 exhibited a similar morphology (Fig. S1A) and similar crystal diffraction (Fig. S1B) as NH_2-MIL-101, but no fluorescence emission at 456 nm was observed (Fig. S1C).

3.2. Ratiometric fluorescence based on the bifunctional NH_2-MIL-101 MOF

Fe-based MOFs are peroxidase mimics that catalyze the oxidation of enzyme-linked substrates, such as OPD, 3,3′,5,5′-tetramethylbenzidine, and 2,2′-azino-bis(3-ethylbenzo-thiazoline-6-sulfonic acid) diammonium salt (Li et al., 2018; Ai et al., 2013; Feng et al., 2012). Among these, OPD is a typical fluorescent substrate. By coupling OPD and NH_2-MIL-101, a ratiometric fluorescence assay can be constructed. As shown in Fig. S2, H_2O_2 had no effect on the fluorescence of NH_2-MIL-101. However, when OPD was introduced, the NH_2-MIL-101 fluorescence (F_{456}) significantly decreased, and a new FL peak at 556 nm (F_{556}) emerged that was attributed to the oxidation product of OPD (Zhao et al., 2016). These results indicated that non-fluorescent OPD was oxidized into fluorescent DAP by H_2O_2 in the presence of NH_2-MIL-101; the DAP also quenched the NH_2-MIL-101 fluorescence. In contrast, when OPD was mixed with H_2O_2 in the absence of NH_2-MIL-101, no F_{556} was observed. This verified the excellent catalytic activity of NH_2-MIL-101 toward OPD oxidation by H_2O_2. Finally, in the absence of H_2O_2, the NH_2-MIL-101/OPD system exhibited no F_{456} change and negligible F_{556}. Photographs of those solutions under UV illumination were shown in the inset of Fig. S2. The NH_2-MIL-101/H_2O_2/OPD system had strong yellow emission that differed from the blue emission of NH_2-MIL-101, NH_2-MIL-101/H_2O_2, and NH_2-MIL-101/OPD systems. Furthermore, no fluorescence emission was observed from the H_2O_2/OPD system. These results were consistent with the fluorescence spectra. The F_{456} and F_{556} intensities before and after the catalytic reaction are presented in Fig. 2A. As shown, high F_{456} and low F_{556} were observed before catalytic reaction while inverse results appeared after catalytic reaction.

The time dependence of F_{456} and F_{556} during the catalytic process was plotted in Fig. 2B, where F_{556} increased and F_{456} decreased over the period 0–30 min. Similar results were observed when altering the OPD or H_2O_2 concentrations. Higher concentrations of either generated more DAP (Fig. S3). These observations confirmed that NH_2-MIL-101 catalyzed OPD oxidation by H_2O_2 to produce DAP, which quenched the fluorescence of NH_2-MIL-101.

To understand the fluorescent quenching mechanism between NH_2-MIL-101 and DAP, zeta potential was measured via laser electrophoresis light scattering technique (See Supplementary Material). This is because it is a measure of the particle surface charge and is defined as the electrical potential at the slip plane (or layer) between the Stern layer and the diffuse layer (Shim et al., 2002). The zeta potential of NH_2-MIL-101 was 15.2 mV at pH 4.0, while DAP had positive charges in acidic solution because of its two amino groups in the phenazine structure. Thus, electrostatic attraction between NH_2-MIL-101 and DAP was unlikely, suggesting only a weak interaction. Fluorescence resonance energy transfer was also excluded because of the weak interaction and the absence of chemical linkage (Yan et al., 2015; Xiao et al., 2018). In Fig. S4, there was a significant overlap between the NH_2-MIL-101 fluorescence and the DAP UV absorption spectra. Thus, the inner-filter effect (IFE) appears to be the main reason for the fluorescence quenching, in which NH_2-MIL-101 was the fluorescence reporter and DAP the quencher (Yan et al., 2015; Liu et al., 2017; Shao et al., 2005). Furthermore, higher DAP (absorber) concentrations induced more IFE (Fig. S3A) because of increased overlaps in DAP adsorption and NH_2-MIL-101 emission (Fig. S4).

3.3. Sensing principle of PPi and ACP via ratiometric fluorescence

PPi readily forms complexes with metal ions. Hence, when it was introduced into the NH_2-MIL-101/H_2O_2/OPD system, it coordinated

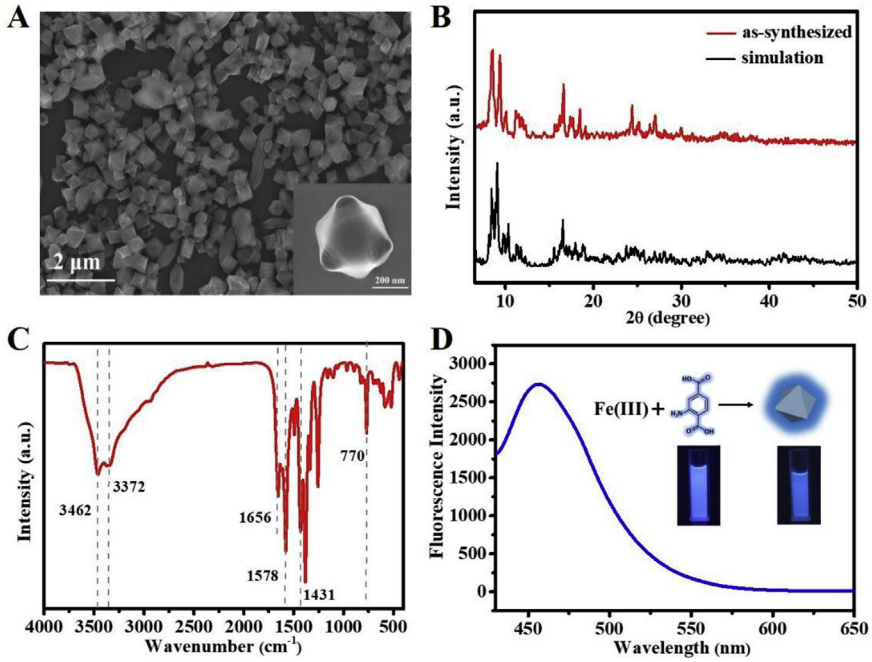

Fig. 1. (A) SEM image of NH_2-MIL-101. Inset shows enlarged image. (B) XRD profiles of NH_2-MIL-101 and simulated MIL-101. (C) FT-IR spectrum of NH_2-MIL-101. (D) Fluorescence spectrum of NH_2-MIL-101 (Inset: schematic of fluorescent NH_2-MIL-101 synthesis; photos of NH_2-BDC and NH_2-MIL-101 under UV excitation).

with the Fe–O cluster in NH_2-MIL-101, inhibiting the catalytic activity on OPD. As shown in Fig. 3A, the NH_2-MIL-101/H_2O_2/OPD system exhibited increased the F_{456} intensity with increasing PPi concentration, while the F_{556} intensity decreased. The PPi-induced decline in NH_2-MIL-101 catalytic activity was confirmed by kinetics shown in Fig. 3B, which plots F_{556}/F_{456} vs. reaction time at different PPi concentrations. The slopes decreased with increasing PPi concentration, suggesting that PPi inhibited the NH_2-MIL-101 catalytic activity.

Because ACP catalyzed the hydrolysis of PPi, the catalytic activity of NH_2-MIL-101 could be recovered by adding ACP to the NH_2-MIL-101/H_2O_2/OPD/PPi system. As shown in Fig. 3A, the DAP fluorescence at 556 nm was restored in the presence of ACP, while the fluorescence of NH_2-MIL-101 at 456 nm was quenched. PPi analogues, such as PO_4^{3-}, HPO_4^{2-}, and $H_2PO_4^{-}$, had negligible effects on both the NH_2-MIL-101/OPD catalysis (Fig. S5A), and the inhibitory behavior of PPi toward NH_2-MIL-101 (Fig. S5B).

3.4. Analytical performance for PPi and ACP sensing

In the absence of PPi analyte, the NH_2-MIL-101/H_2O_2/OPD system exhibited a ratiometric fluorescence spectrum with negligible F_{456} and distinct F_{556}. As noted above, F_{456} increases and F_{556} decreases with PPi. Fluorescent spectra at different concentrations of PPi ranging over 0–25 μM are shown in Fig. 4A. In Fig. 4B, F_{556}/F_{456} decreased with increasing PPi concentration, where a linear relationship was obtained in the range 0–10 μM (inset of Fig. 4B) and was fitted by $F_{556}/F_{456} = 4.4463–0.3991$ [PPi], with $r^2 = 0.9922$ ($n = 15$). This indicated a feasible assay for PPi. To test the specificity of PPi detection, selectivity experiments were conducted by comparing F_{556}/F_{456} of the blank with values in the presence of potentially interfering anions, including F^-, Cl^-, Br^-, I^-, NO_3^-, Ac^-, CO_3^{2-}, and SO_4^{2-}, in the absence and presence of PPi (see Fig. S6). Distinct changes in F_{556}/F_{456} were observed only in the presence of PPi, and the presence of other anions had no effects.

Adopting PPi as a mediator, the ratiometric fluorescence probe was further developed for screening ACP activity. PPi would be hydrolyzed by the ACP, leading to the fluorescent recovery of the PPi/NH_2-MIL-101/H_2O_2/OPD system. Fluorescence spectra of the sensing system vs. ACP concentration over the range 0–100 U/L are shown in Fig. 4C. With increasing ACP concentration, F_{456} decreased and F_{556} increased. A linear relationship of F_{556}/F_{456} vs. ACP concentration was observed over the concentration range of 0.01–30 U/L (inset of Fig. 4D), which was fitted by $F_{556}/F_{456} = 0.7358 + 0.1186$ [ACP], with $r^2 = 0.9941$ ($n = 12$). The detection limit was 0.005 U/L (S/N = 3), which was

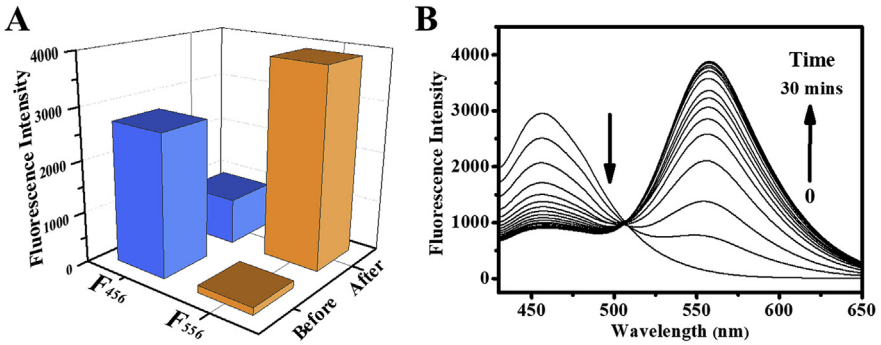

Fig. 2. (A) 3D equivalent columns of fluorescence intensities at 456 nm and 556 nm before and after catalysis. (B) Fluorescence spectrum of NH_2-MIL-101/H_2O_2/OPD system vs. reaction time (0, 2, 4, 6, 8, 10, 12, 14, 16, 18, 20, 22, 24, 26, 28, 30 min).

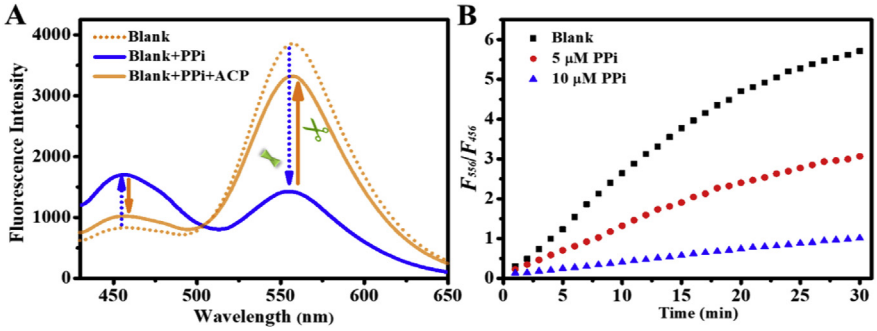

Fig. 3. (A) Fluorescence spectra of the NH_2-MIL-101/H_2O_2/OPD, NH_2-MIL-101/H_2O_2/OPD/PPi, and NH_2-MIL-101/H_2O_2/OPD/PPi/ACP systems. (B) F_{556}/F_{456} vs. reaction time for different PPi concentrations in the NH_2-MIL-101/H_2O_2/OPD system.

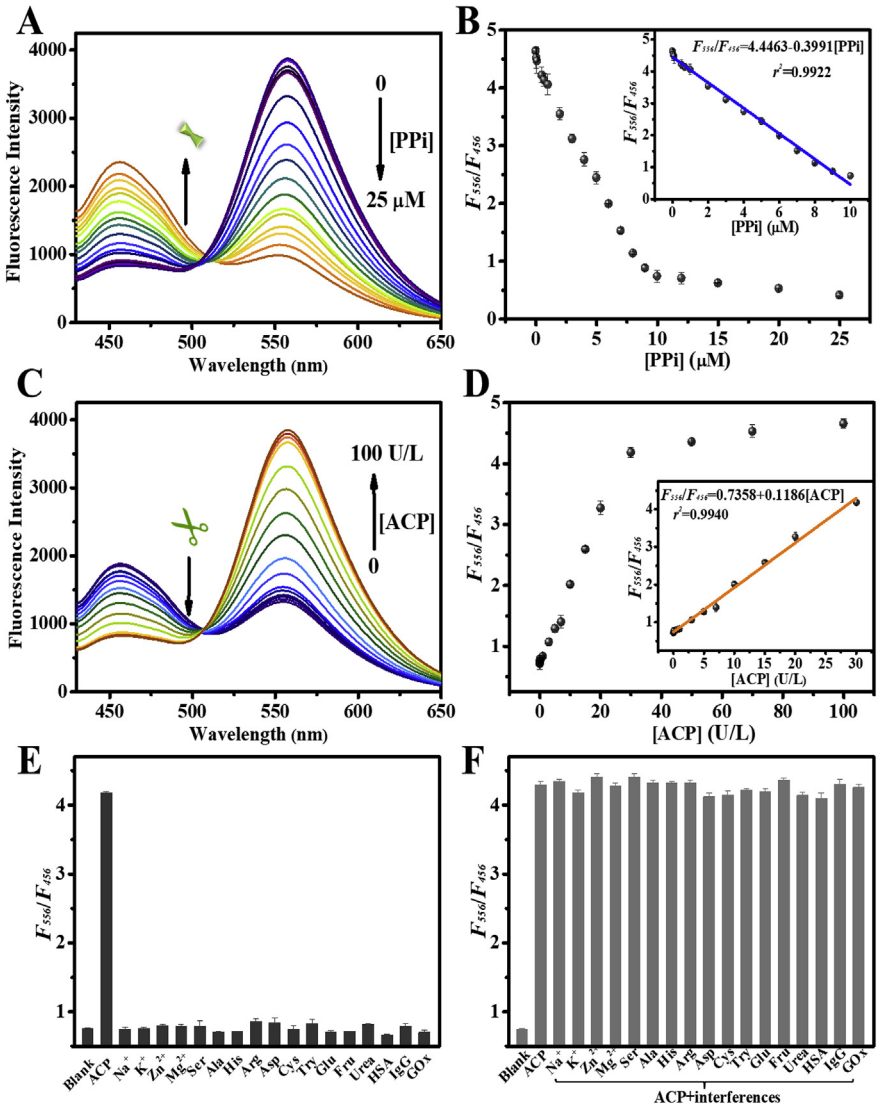

Fig. 4. (A) Fluorescence spectra of the NH_2-MIL-101/H_2O_2/OPD system in the presence of different concentrations of PPi (0–25 μM). (B) F_{556}/F_{456} values vs. PPi concentration. Inset: linear relationship between F_{556}/F_{456} and PPi concentration in the 0–10 μM range. (C) Fluorescence spectra of the NH_2-MIL-101/H_2O_2/OPD/PPi system in the presence of different concentrations of ACP (0–100 U/L). (D) F_{556}/F_{456} vs. ACP concentration. Inset: linear relationship between F_{556}/F_{456} vs. ACP concentration in the 0.01–30 U/L range. (E) Effects of other substances on F_{556}/F_{456} for the NH_2-MIL-101/H_2O_2/OPD/PPi system. The concentrations of ACP, GOx, IgG, HAS, and the other substances were 30 U/L, 50 U/L, 1 mg/mL, 0.1 mg/mL, and 10 μM, respectively. (F) Effects of other substances on F_{556}/F_{456} for the NH_2-MIL-101/H_2O_2/OPD/PPi system in the presence of ACP. The concentrations of ACP, GOx, IgG, HAS, and the other substances were 30 U/L, 50 U/L, 1 mg/mL, 0.1 mg/mL, and 10 μM, respectively.

comparable to or better than that for other probes (Table S1), such as nitrogen-doped graphene quantum dots (0.014 U/L, Qu et al., 2018), graphene quantum dots (0.028 U/L, Na et al., 2016), a thick-film magneto-elastic transducer (1.5 U/L, Wu et al., 2007), carbon quantum dots (5.5 U/L, Qian et al., 2015), and luminescent aggregated copper nanoclusters (1.3 U/L, Huang et al., 2016). Furthermore, a much broader linear range of this method is expected for other applications.

To test the ACP detection selectivity, the effects of various targets on the FL response of the PPi/NH_2-MIL-101/H_2O_2/OPD system were studied. These include biologically relevant metal ions (Na^+, K^+, Zn^{2+}, Mg^{2+}), amino acids (Ser, Ala, His, Arg, Asp, Cys, Try), proteins (HAS, IgG and GOx), and others (Glu, Fru and Urea). The results in Fig. 4E indicated that only ACP produced significant changes in F_{556}/F_{456} values, while the presence of the other targets had negligible effects. As shown in Fig. 4F, F_{556}/F_{456} values for ACP detection remained unchanged in the presence of potential interferences, confirming the selective assay in the complex matrix. Overall, the results demonstrated that the method was highly selective for ACP detection.

3.5. ACP detection in human serum samples

To demonstrate the potential of the ACP assay in complex biological samples, the recovery tests were performed on a three diluted human serum samples. As shown in Table S2, the recoveries for the spiked samples ranged from 97.1% to 104.2% with RSD (relative standard deviation) values of 1.0%–4.3%. The repeatability and reproducibility of the F_{556}/F_{456} ratio for fixed concentrations of 5 U/L ACP and 10 μM PPi in the serum samples were examined. Seven repeated measurements of 5 U/L ACP were performed for the same human serum sample under optimized conditions to evaluate repeatability. In Table S3, the RSD was 3.1%, revealing good repeatability. The reproducibility was evaluated by detecting 5 U/L ACP in five different human serum samples. In Table S4, the RSD was 4.0%, showing good reproducibility. Overall, the results indicated feasibility of this ratiometric fluorescent sensor for ACP detection in real biological samples.

3.6. Application to a cascade logic gate

Molecular logic gates may enable molecular-scale computers and "autonomously regulated" chemical systems. Various logic gates have attracted extensive interest for intelligent biosensing and diagnostics (Fan et al., 2017; Lin et al., 2011, 2018; Huang et al., 2011). Here, the PPi/ACP–mediated fluorescence changes in the NH_2-MIL-101/H_2O_2/OPD system could be used as a cascade INHIBIT logic gate; the equivalent circuit is presented in Fig. 5A. For the first decoder, PPi and ACP were the two inputs and the presence of PPi or ACP was defined as "1" and their absence as "0". The output of the first decoder was defined as "1" when complete PPi existed after incubation. Other outputs (including buffer, ACP, and mixture of ACP and phosphate group) were defined as "0". The output of first decoder was utilized as the input of second decoder that consisted of the mixture NH_2-MIL-101, H_2O_2, and OPD as the platform. The final outputs of the cascade logic gate were F_{456} and F_{556}, and the threshold values were respectively set to "1100" and "1500" (half of the corresponding maximum value) to judge the 1/0 signal. The F_{456} and F_{556} column bars against various input combinations and the corresponding truth table are shown in Fig. 5B and C, respectively. With no input of PPi and ACP (input "0, 0"), OPD was oxidized by H_2O_2, as catalyzed by NH_2-MIL-101, to produce fluorescent DAP. The NH_2-MIL-101 F_{456} decreased, while DAP F_{556} increased, giving an output signal of "0" for F_{456} and "1" for F_{556} (output "0, 1"). With the ACP input alone (input "0, 1"), OPD was still oxidized by H_2O_2, and the output of F_{456} was "0" and F_{556} was "1" (output "0, 1"). With the PPi input alone (input "1, 0"), the catalytic ability of NH_2-MIL-101 was inhibited. NH_2-MIL-101 F_{456} increased, while DAP F_{556} decreased, giving an output signal of "1" for F_{456} and "0" for F_{556} (output "1, 0"). With PPi and ACP together (input "1, 1"), PPi was hydrolyzed into a phosphate group by ACP, thus the catalytic ability of NH_2-MIL-101 was recovered. The NH_2-MIL-101 F_{456} decreased, while DAP F_{556} increased, giving an output signal of "0" for F_{456} and "1" for F_{556} (output "0, 1").

4. Conclusion

In conclusion, a ratiometric fluorescence sensor for PPi and ACP, based on bifunctional NH_2-MIL-101 MOFs, was demonstrated. As a peroxidase mimic catalyst, the NH_2-MIL-101 accelerated H_2O_2 oxidization of OPD to produce fluorescent DAP, which then quenched F_{456} emission from the NH_2-MIL-101 MOFs. The inner filter effect between NH_2-MIL-101 MOFs and DAP was mainly responsible for the quenching. Because of its specific binding to Fe centers in NH_2-MIL-101, the PPi-induced decrease in the NH_2-MIL-101 catalytic activity in OPD oxidation, and the specific hydrolysis of PPi by ACP, the ratiometric fluorescence enabled sensitive and selective detection of ACP activity. The ratiometric sensor exhibited a wide linear range (0.01–30 U/L), high sensitivity (LOD = 0.005 U/L), and good selectivity for ACP detection. The protocol was used to successfully analyze ACP activity in spiked biological samples of human serum. PPi/ACP-mediated fluorescence changes in the NH_2-MIL-101/H_2O_2/OPD system also enabled a functioning cascade INHIBIT logic gate. It is anticipated that such a new strategy based on luminescence and biomimetic catalytic activity of bifunctional LMOFs could enable promising applications in biological analysis and clinical diagnostics.

CRediT authorship contribution statement

Siqi Li: Conceptualization, Methodology, Investigation, Formal analysis, Writing - original draft. **Xue Hu:** Methodology, Formal analysis. **Qiumeng Chen:** Formal analysis, Validation. **Xiaodan Zhang:** Formal analysis, Validation. **Hongxiang Chai:** Formal analysis, Writing - review & editing. **Yuming Huang:** Conceptualization, Formal analysis, Writing - review & editing, Supervision.

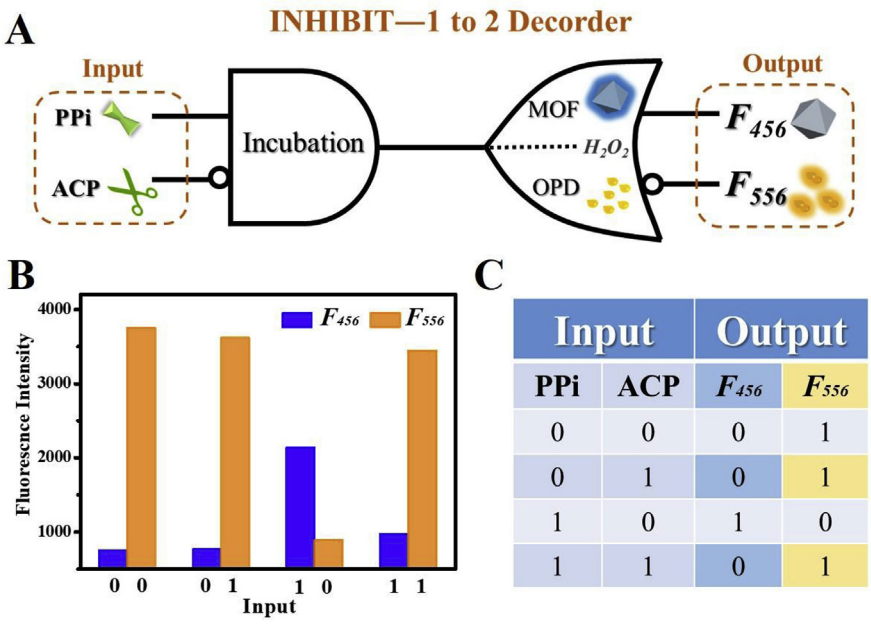

Input		Output	
PPi	ACP	F_{456}	F_{556}
0	0	0	1
0	1	0	1
1	0	1	0
1	1	0	1

Fig. 5. (A) Equivalent logic representation of the cascade logic gate, an INHIBIT gate cascade with 1–2 decoder, in which the F_{456} and F_{556} are two final outputs. (B) Fluorescence column bars for simultaneous F_{456} (blue columns) and F_{556} (orange red columns) under different input variations. (C) Truth table of the cascade logic gate (PPi concentration was 10 μM). (For interpretation of the references to color in this figure legend, the reader is referred to the Web version of this article.)

Acknowledgment

Financial support from the National Natural Science Foundation of China (No. 51678485) is gratefully acknowledged. We thank Dr. Alan Burns, from the Liwen Bianji, Edanz Group China (www.liwenbianji.cn/ac), for editing the English text of a draft of this manuscript.

Appendix A. Supplementary data

Supplementary data to this article can be found online at https://doi.org/10.1016/j.bios.2019.05.010.

References

Ai, L., Li, L., Zhang, C., Fu, J., Jiang, J., 2013. Chem. Eur J. 19, 15105–15108.
Allendorf, M.D., Bauer, C.A., Bhakta, R.K., Houk, R.J.T., 2009. Chem. Soc. Rev. 38, 1330–1352.
Barbosa, A.D.S., Julião, D., Fernandes, D.M., Peixoto, A.F., Freire, C., Castro, B.de, Granadeiro, C.M., Balula, S.S., Cunha-Silva, L., 2017. Polyhedron 127, 464–470.
Bauer, S., Serre, C., Devic, T., Horcajada, P., Marrot, J., Fe´rey, G., Stock, N., 2008. Inorg. Chem. 47, 7568–7576.
Cui, Y., Yue, Y., Qian, G., Chen, B., 2012. Chem. Rev. 112, 1126–1162.
Deng, H.H., Lin, X.L., Liu, Y.H., Li, K.L., Zhuang, Q.Q., Peng, H.P., Liu, A.L., Xia, X.H., Chen, W., 2017. Nanoscale 9, 10292–10300.
Fan, D., Shang, C., Gu, W., Wang, E., Dong, S., 2017. ACS Appl. Mater. Interfaces 9, 25870–25877.
Feng, D., Gu, Z.Y., Li, J.R., Jiang, H.L., Wei, Z., Zhou, H.C., 2012. Angew. Chem. 124, 10453–10456.
Gkaniatsou, E., Sicard, C., Ricoux, R., Mahy, J., Steunou, N., Serre, C., 2017. Mater. Horiz. 4, 55–63.
Gong, D., Han, S.C., Iqbal, A., Qian, J., Cao, T., Liu, W., Liu, W., Qin, W., Guo, H., 2017. Anal. Chem. 89, 13112–13119.
Hu, Z., Deibert, B.J., Li, J., 2014. Chem. Soc. Rev. 43, 5815–5840.
Huang, W.T., Shi, Y., Xie, W.Y., Luo, H.Q., Li, N.B., 2011. Chem. Commun. 47, 7800–7802.
Huang, Y., Feng, H., Liu, W., Zhou, Y., Tang, C., Ao, H., Zhao, M., Chen, G., Chen, J., Qian, Z., 2016. Anal. Chem. 88, 11575–11583.
Jiao, L., Wang, Y., Jiang, H.L., Xu, Q., 2018. Adv. Mater. 30 1703663.
Kathryn, M.L.T. Pashow, Rocca, J.D., Xie, Z., Tran, S., Lin, W., 2009. J. Am. Chem. Soc. 131, 14261–14263.
Kong, H.Y., Byun, J., 2013. Biomol. Ther. 21, 10–20.
Kreno, L., Leong, K., Farha, O.K., Allendorf, M., Van Duyne, R.P., Hupp, J.T., 2012. Chem. Rev. 112, 1105–1125.
Lee, M.H., Kim, J.S., Sessler, J.L., 2015. Chem. Soc. Rev. 44, 4185–4191.
Lei, J., Qian, R., Ling, P., Cui, L., Ju, H., 2014. Trac. Trends Anal. Chem. 58, 71–78.
Li, X., Guo, W., Liu, Z., Wang, R., Liu, H., 2017. J. Hazard Mater. 324, 665–672.
Li, S., Liu, X., Chai, H., Huang, Y., 2018. Trac. Trends Anal. Chem. 105, 391–403.
Lin, Y., Tao, Y., Pu, F., Ren, J., Qu, X., 2011. Adv. Funct. Mater. 21, 4565–4572.
Lin, X., Liu, Y., Deng, J., Lyu, Y., Qian, P., Li, Y., Wang, S., 2018. Chem. Sci. 9, 1774.
Liu, J.W., Luo, Y., Wang, Y.M., Duan, L.Y., Jiang, J.H., Yu, R.Q., 2016. ACS Appl. Mater. Interfaces 8, 33439–33445.
Liu, H., Li, M., Xia, Y., Ren, X., 2017. ACS Appl. Mater. Interfaces 9, 120–126.
Na, W., Liu, Q., Sui, B., Hu, T., Su, X., 2016. Talanta 161, 469–475.
Nath, I., Chakrabort, J., Verpoort, F., 2016. Chem. Soc. Rev. 45, 4127–4170.
Qian, Z., Chai, L., Zhou, Q., Huang, Y., Tang, C., Chen, J., Feng, H., 2015. Anal. Chem. 87, 7332–7339.
Qu, Z., Na, W., Liu, X., Liu, H., Su, X., 2018. Anal. Chim. Acta 997, 52–59.
Seki, K., Miyakoshi, S., Lee, G.H., Matsushita, H., Mutoh, Y., Nakase, K., Ida, M., Taniguchi, H., 2004. Am. J. Surg. Pathol. 28, 1384–1388.
Shao, N., Zhang, Y., Cheung, S.M., Yang, R.H., Chan, W.H., Mo, T., Li, K.A., Liu, F., 2005. Anal. Chem. 77, 7294–7303.
Shim, Y., Lee, H.-J., Lee, S., Moon, S.-H., Cho, J., 2002. Environ. Sci. Technol. 36, 3864–3871.
Srikun, D., Miller, E.W., Domaille, D.W., Chang, C.J., 2008. J. Am. Chem. Soc. 130, 6718–6719.
Stavitski, E., Goesten, M., Juan-AlcaÇiz, J., Martinez-Joaristi, A., Serra-Crespo, P., Petukhov A, V., Gascon, J., Kapteijn, F., 2011. Angew. Chem. Int. Ed. 50, 9624–9628.
Sun, J., Yang, F., Yang, X., 2015. Nanoscale 7, 16372–16380.
Teng, Y., Jia, X., Li, J., Wang, E., 2015. Anal. Chem. 87, 4897–4902.
Wang, J., Yan, Y., Yan, X., Hu, T., Tang, X., Su, X., 2016. Sens. Actuators, B 234, 470–477.
Wu, S., Gao, X., Cai, Q., Grimes, C.A., 2007. Sens. Actuators, B 123, 856–859.
Wu, B., Lin, X., Ge, L., Wu, L., Xu, T., 2013. Chem. Commun. 49, 143–145.
Xiao, T., Sun, J., Zhao, J., Wang, S., Liu, G., Yang, X., 2018. ACS Appl. Mater. Interfaces 10, 6560–6569.
Xu, Y., Li, B., Xiao, L., Ouyang, J., Sun, S., Pang, Y., 2014. Chem. Commun. 50, 8677–8680.
Yam, L.T., 1974. Am. J. Med. 56, 604–616.
Yan, X., Li, H., Han, X., Su, X., 2015. Biosens. Bioelectron. 74, 277–283.
Yi, F.Y., Chen, D., Wu, M.K., Han, L., Jiang, H.L., 2016. ChemPlusChem 81, 675–690.
Zhang, Z., Li, X., Liu, B., Zhao, Q., Chen, G., 2016. RSC Adv. 6, 4289–4295.
Zhao, C., Jiang, Z., Mu, R., Li, Y., 2016. Talanta 159, 365–370.
Zhao, L., Xie, S., Song, X., Wei, J., Zhang, Z., Li, X., 2017. Biosens. Bioelectron. 91, 217–224.
Zhou, H.-C., Kitagawa, S., 2014. Chem. Soc. Rev. 43, 5415–5418.